Chapter 4

Power Flow Algorithms for Islanded Microgrids

4.1 Introduction

The PF analysis of DCIMGs is a growing research area. Several algorithm have been proposed to solve the PF problem of the DCIMG. The conventional PF techniques have issues in handling DCIMG due to the nonexistence of reference bus (slack bus) in the system. To address this issue, different novel algorithms are proposed in this chapter for solving the PF problem of DCIMG.

The smart grid architecture based electrical distribution systems are mainly distinguished by higher penetration of DGs. In microgrids, this increasing penetration of DGs with adequate generation can bear the active and reactive power requirement for all or most of its local loads. According to US Department of Energy definition of a microgrid "A group of interconnected loads and distributed energy resource within clearly defined electrical boundaries that acts as a single controllers entity with respect to the grid and that connects [to] and disconnects from such [a] grid to enable it to operate in both grid-connected and island mode" [160].

For the operational analysis of microgrid, there is a requirement of suitable PF tool. In islanded microgrid system, operating frequency value is not constant thus frequency is also a PF variable and Ybus is also not constant due to the reactance of the lines being frequency dependent [93, 161–163]. In a conventional grid-connected system, DGs buses are working as a PQ or PV buses and the excess power is fed from the slack

bus [56,94,95,164]. But such phenomena are not applicable in the islanded system because there is no slack bus in the system. Thus, conventional PF method is not applicable in islanded microgrid [165, 166].

To determine the PF solution for DCIMG, new algorithms have been introduced. These techniques have considered linear equations of the droop characteristics of DGs. The NTR method has been proposed [56] to solve equations obtained after consolidating (i) linear droop bus equations, and (ii) PF equation. In [94], a new PF method that employs PSO is introduced to solve the PF problem of DCIMG. The modified NR method has been used in [2] to solve the power flow problem of DCIMG.

In literature, several works address the power flow problem of a DCIMG. However, these works cannot be applied effectively to the PF problem of DCIMG.

This chapter proposes new algorithms for solving the PF problem of DCIMG using different approaches. In these approaches, any droop bus is considered as an Angle Reference (AR) bus and voltage magnitude of this AR bus and operating system frequency are updated according to the droop characteristics of DGs in the outer loop of the algorithms. Voltages of all buses except AR bus are updated in every iteration by solving the non-linear current-injection based power flow equations. To verify the execution of the proposed power flow approaches on power flow problem of a DCIMG, the outcomes have been compared with the outcomes of optimization algorithm NTR [56], PSCAD [167], MNR algorithm, Direct Backward/Forward Sweep (DBFS) algorithm , and Modified Backward/Forward Sweep (MBFS) algorithm [2].

To sum up, the major contributions of the present work are as follows:

1. This chapter proposes current-injection based NR algorithm, and Nested Backward/Forward Sweep (NBFS) algorithm to solve the PF problem of DCIMG.

2. The proposed algorithms overcome the issues and limitations of NR-based algorithms MNR and NTR, and the need for a gradient of the Ybus with respect to frequency in the Jacobian matrix. The proposed algorithm updates the system frequency in every loop without using the gradient of the Ybus or any other variable with respect to frequency.

3. A closed loop formulation is proposed to evaluate the values of voltage magnitude of AR bus and system frequency, which results in fast convergence in the algorithm.

4. In this chapter, approach of closed loop design has been investigated for convergence through various tests, designed for the purpose.

5. This chapter also investigates the robustness and efficacy of the proposed algorithm for ill-conditional test systems having higher loading conditions and r/x ratios.

4.2 Modeling of Distributed Generations and Different Loads

The modeling of the system components influences the PF solutions. The models of DG and loads are presented in the following subsection.

4.2.1 Modeling of Distributed Generation

The penetration of DGs has been increasing commonly in the distribution systems. A wide category of technologies viz. wind turbines, photovoltaic systems, energy storage systems, fuel cells, and micro-turbines have been incorporated as types of DGs. Consequently, there is a requirement of modeling schemes to handle these DGs in the power flow analysis of DCIMG systems. The electrical characteristics of DGs are based on energy converter utilized in them. The different models for DG are proposed in literature based on electrical characteristics such as constant voltage model (PV), voltage-dependent power factor model (PQ(v)), constant current model (PI), and constant power factor model (PQ), as shown in Table 4.1. In a DCIMG operating mode, these DG units with battery energy storage systems and droop controllers are designed to control the system frequency and voltage while sharing the load demand [168]. In DCIMGs, droop-controlled DG units are designed to imitate the droop characteristics of synchronous generators operating in parallel. Generally, conventional droop settings are capable of providing accurate power-sharing among DG units in DCIMGs.

To model the DGs, based on the output impedance seen by the DGs and r/x ratio of the line, three different droop equations (conventional droop, inverse droop and mixed droop) are considered [104,105]. For the inductive network, DGs operating in conventional droop [163, 169] can be modelled as:

$$|V_k| = |V_{0,k}| - n_k(Q_{G,k} - Q_{0,k}) \tag{4.1}$$

Table 4.1: Component modelling of microgrid in Power Flow algorithm

Primary Energy Resource	Energy Conv.	Model	
		Grid Connected	Islanded
Wind turbine	Double feed induc. gen.	PQ	droop
	Syn. Gen. (Slip control)	PQ	droop
Photo-voltaic system	Current/voltage controlled inverter	PV	droop
Fuel cell	St. pwr. conv. (voltage controlled)	PV	droop
CHP	St. pwr. conv. (power factor controlled)	PQ	droop
	St. pwr. conv. (voltage controlled)	PV	droop
Energy storage	St. pwr. conv. (voltage controlled)	PV	droop
Gas Turbine	St. pwr. conv. (voltage controlled)	PV	droop
Microturbine	Induc. Gen. + St. pwr. conv.	PQ	droop
Geothermal/Ocean Energy/ I.C Engine	Syn. Gen. (Constant Excit. Voltage)	PQ	droop

$$\omega = \omega_0 - m_k(P_{G,k} - P_{0,k}) \tag{4.2}$$

where,

$P_{G,k}$ and $Q_{G,k}$ are the active and reactive power output of k^{th} DG respectively. n_k and m_k are the voltage and frequency droop coefficients of k^{th} DG respectively. $Q_{0,k}$ and $P_{0,k}$ are the power set points at k^{th} DG respectively.

For the resistive network, DGs operating in inverse droop [170, 171] can be modelled as:

$$|V_k| = |V_{0,k}| - n_k(P_{G,k} - P_{0,k}) \tag{4.3}$$

$$\omega = \omega_0 - m_k(Q_{G,k} - Q_{0,k}) \tag{4.4}$$

In practical applications, different DGs can be located a little far from each other and can be paralleled through lines, which contain significant line impedances. The performance of above-mentioned droop characteristics (for fully resistive and fully inductive case) is not satisfactory in case complex impedance and power-sharing among the DGs is not efficient due to active and reactive power coupling. Hence, a mixed droop characteristics [104, 105] is considered. Modelling of DG operating in mixed droop can be expresses as;

$$|V_k| = |V_{0,k}| - n_k(P_{G,k} + Q_{G,k}) \tag{4.5}$$

$$\omega = \omega_0 - m_k(P_{G,k} - Q_{G,k}) \tag{4.6}$$

A dominant DG (typically synchronous generator based DGs) can be operated in isochronous mode, thereby functioning as a non-ideal slack bus i.e., providing constant

frequency and voltage at its terminals regardless of the connected load. Other DGs can operate according to their droop settings. To model isochronously controlled DG, the same droop equations can be adopted by setting droop coefficients to zero, i.e., $|V_k| = |V_{0,k}|$ and $\omega = \omega_0$.

In this chapter, two parameter x and y are considered to obtain all above-mentioned four droop equation of DGs in single composite droop equation. This single composite droop equation can be written as follows:

$$\omega = \omega_0 - m_k(x_k(P_{G,k} - P_{0,k}) - y_k(Q_{G,k} - Q_{0,k})) \tag{4.7}$$

$$|V_k| = |V_{0,k}| - n_k(y_k(x_k(P_{G,k} - P_{0,k}) + x_k(Q_{G,k} - Q_{0,k})) \tag{4.8}$$

In equations (4.7) and (4.8), values of x and y are considered to be either 1 or 0. Hence, there are four possible combination of x and y and each combination represents different droop operation of DGs. If $x = 1$ and $y = 0$, the droop equations are reduced to equations 4.1 and 4.2 i.e. the conventional droop. While $\{x, y\} = \{0, 1\}$ and $\{x, y\} = \{1, 1\}$ represents the inverse droop and mixed droop operation respectively. The last combination, $\{x, y\} = \{0, 0\}$, represents that the DG is acting either as a isochronously controlled or it is operating in grid connected system.

4.2.2 Load Modelling

In static load model, active and reactive power absorbed by the load depends upon the bus voltage and system frequency. Voltage and frequency based active and reactive loads can be represented as given in equations (4.9) and (4.10) respectively.

$$P_{l,k} = P_{0,l,k}(a_p + b_p|V_k| + c_p|V_k|^2 + d_p|V_k|^{\alpha})(1 + e_p(\omega - \omega_0)) \tag{4.9}$$

$$Q_{l,k} = Q_{0,l,k}(a_q + b_q|V_k| + c_q|V_k|^2 + d_q|V_k|^{\beta})(1 + e_q(\omega - \omega_0)) \tag{4.10}$$

where, $a_p + b_p + c_p + d_p = 1$ and $a_q + b_q + c_q + d_q = 1$; ω_0 is the nominal system frequency; e_p and e_q are the frequency dependability coefficient for active and reactive load respectively; ω is the operating system frequency; $P_{0,l,k}$ and $Q_{0,l,k}$ are active and reactive load demand at bus k, when system is operating at nominal frequency and bus voltage; α and β are the active and reactive power exponents respectively.

Nowadays, a large number of Plug-in Hybrid Electric Vehicles (PHEVs) are connected to the modern distribution system. The influence of PHEV loads can be estimated by using different models based on their electrical characteristics which are mainly depended on their different charging operations of the chargers. In this chapter, three different voltage-dependent load models of PHEVs are considered for power flow analysis of DCIMG.

The first type of PHEV load model is represented by a polynomial load (PHEVI) model. In PHEVI, active and reactive power are represented by the following equations.

$$P_{EVI,k} = P_{0,EVI,k}(a_p + b_p|V_k| + c_p|V_k|^2), \tag{4.11}$$

and

$$Q_{EVI,k} = Q_{0,EVI,k}(a_q + b_q|V_k| + c_q|V_k|^2). \tag{4.12}$$

PHEVI has coefficients a_q, b_q, and c_q for the reactive power and a_p, b_p, and c_p for the active power.

In case of the second type of PHEV load model, active power and reactive power are represented by using equations 4.13 and 4.14, respectively considering fast charging station as defined in [172].

$$P_{EVII,k} = P_{0,EVII,k}(a_p + b_p|V_k|^{\alpha}), \text{and} \tag{4.13}$$

$$Q_{EVII,k} = P_{EVII,k}tan(\theta), \tag{4.14}$$

where, a, b, and α represent power constant, exponent constant, and exponent of the voltage magnitude, respectively.Parameter θ is power factor which is equal to 0.97 [172].

The third type of PHEV load model, PHEVIII, is represented by the constant current load. In this case, reactive power and active power are obtained by using polynomial load model, where $P_{EVIII,k}$ of PHEVIII is calculated as follows.

$$P_{EVIII,k} = P_{0,EVIII,k}|V_k|^2, \text{and} \tag{4.15}$$

reactive power,

$$Q_{EVIII,k} = 0. \tag{4.16}$$

The above defined PHEV load models can be handled by using equations (4.9) and (4.10).

4.3 Current Injection Newton-Raphson Algorithm for DCIMG

In this section, a novel algorithm, called CINR, is introduced to solve the PF problem of DCIMG.

In the case of DCIMGs, conventional PF techniques cannot solve the PF problem to provide the steady-state value of system variables for further investigation. In MNR and NTR, some elements of the Jacobian matrix contain the derivative of elements of the bus admittance matrix with respect to the frequency. Reference [2] (where MNR is proposed) provides a brief description of the calculation procedure of the Jacobian matrix. However, in [2], the mutual coupling of the line parameter has not been addressed in the computation procedure of derivative of elements of the bus admittance matrix. In the case of DCIMG having a mutual coupling of the line parameter, we cannot calculate the derivative of the admittance matrix analytically. In such cases, finite difference approximation of the derivatives can be used in place of the analytical derivative, but finite difference step size is to be chosen properly so that the convergence property of Newton-based algorithms [173] is maintained. Various methods have been proposed to select the value of finite difference step-size [173], but these methods increase the time and space complexity of the algorithm and it may also be impractical to solve the power flow problem of a large DCIMG system using these algorithms.

It is interesting to note that non-derivative based PF techniques, DBFS [98] and MBFS [174], are also proposed to solve the power flow problem of DCIMG and they use inner and outer loop approach to update the frequency and voltage magnitude of the slack bus. A similar approach, loop-based frequency update technique, is also given with NR algorithm in [101] to solve the PF problem of DCIMG, but this approach cannot handle the high r/x ratio of the lines.

It is observed that an update of the system frequency separately outside the structure of NR-based algorithms provides better performance on PF problem for DCIMG system having mutually coupled line as compared to the finite difference based approaches. However, a robust and efficient approach for updating the system frequency has not been investigated for existing NR-based algorithms for PF problem of DCIMG system having mutually coupled line impedances. So a new NR-based algorithm, called CINR, with a

loop-based approach to update the frequency is proposed in this work to address this issue.

4.3.1 Classification of Bus-Types

In order to formulate the PF formulation of DCIMG, the primary step is to classify the buses operating in the system. In proposed formulation, classification of buses as follows.

1. Droop bus: The buses where droop controlled DGs are connected.
2. AR bus: One of the droop buses is selected as AR bus.
3. PQ bus: The buses where active and reactive powers are known.
4. PV bus: The buses where voltage magnitude and active power are known.

It is to be noted that an AR bus is needed to provide a reference for the voltage angles of the other buses; voltage angle of AR bus is assummed zero.

4.3.2 Current-injection based Power Flow Formulation

The current mismatch equations are given as follows.

$$\triangle I_{r,i} = \sum_{i=1}^{Nbus} (G_{ij}V_{r,j} - B_{ij}V_{m,j}) - \frac{V_{r,i}P_k^{sp} + V_{m,i}Q_k^{sp}}{V_{r,i}^2 + V_{m,i}^2} = 0 \tag{4.17}$$

$$\triangle I_{m,i} = \sum_{i=1}^{Nbus} (B_{ij}V_{r,j} + G_{ij}V_{m,j}) - \frac{V_{m,i}P_k^{sp} - V_{r,i}Q_k^{sp}}{V_{r,i}^2 + V_{m,i}^2} = 0 \tag{4.18}$$

where P_k^{sp} and Q_k^{sp} are the specified real and reactive power injection at bus k respectively. G_{ij} and B_{ij} are the real and imaginary part of the $\{i,j\}^{th}$ element of bus admittance matrix $(Y - bus)$. While, $V_{r,j}$ and $V_{m,j}$ are respectively the real and imaginary part of voltage of the j^{th} bus . Assuming the slack bus as an AR bus, the current mismatches are calculated for the remaining buses as follows:

$$\triangle = [\triangle I_r^T \triangle I_m^T]^T \tag{4.19}$$

Calculation procedure of $\triangle I_r$ and $\triangle I_m$ for different types of buses is given in [22]. To calculate the Jacobian matrix, equations (4.17) and (4.18) are differentiated with respect

to real and imaginary part of all the bus voltages. For system having all four type of buses, the Jacobian matrix, J, is represented as follows.

$$J = \begin{bmatrix} J_{dr-dr} & J_{dr-pq} & J_{dr-pv} \\ J_{pq-dr} & J_{pq-pq} & J_{pq-pv} \\ J_{pv-dr} & J_{pv-pq} & J_{pv-pv} \end{bmatrix} \tag{4.20}$$

The elements of sub-matrices of the Jacobian matrix are given in Table (4.2). After

Table 4.2: Representation of elements of Jacobian Matrix

Diagonal Element	
J_{dr-dr}	$J1 = G_{kk} - \frac{P_{g,k}(V_{m,k}^2 - V_{r,k}^2) - 2V_{r,k}V_{m,k}Q_{g,k}}{V_k^4} - \frac{V_{r,k}}{V_k^3}\left(\frac{y_k V_{r,k}}{m_k x_k^2 + n_k y_k^2} + \frac{x_k V_{m.k}}{n_k x_k^2 - m_k y_k^2}\right)$
	$J2 = -B_{kk} - \frac{Q_{g,k}(V_{r,k}^2 - V_{m,k}^2 - 2V_{r,k}V_{m,k}P_{g,k})}{V_k^4} - \frac{V_{m,k}}{V_k^3}\left(\frac{y_k V_{r,k}}{m_k x_k^2 + n_k y_k^2} + \frac{x_k V_{m,k}}{n_k x_k^2 - m_k y_k^2}\right)$
	$J3 = B_{kk} - \frac{Q_{g,k}(V_{r,k}^2 - V_{m,k}^2) - 2V_{r,k}V_{m,k}P_{g,k}}{V_k^4} - \frac{V_{m,k}}{V_k^3}\left(\frac{y_k V_{m,k}}{m_k x_k^2 + x_k y_k^2} - \frac{x_k V_{r,k}}{n_k x_k^2 - m_k y_k^2}\right)$
	$J4 = G_{kk} - \frac{P_{g,k}(V_{r,k}^2 - V_{m,k}^2) + 2V_{r,k}V_{m,k}Q_{g,k}}{V_k^4} - \frac{V_{r,k}}{V_k^3}\left(\frac{y_k V_{m,k}}{m_k x_k^2 + n_k y_k^2} - \frac{x_k V_{r,k}}{n_k x_k^2 - m_k y_k^2}\right)$
J_{pq-pq}	$J_1 = G_{kk} - \frac{(P_k^{sp})(V_{mk}^2 - V_{rk}^2) - 2V_{rk}V_{mk}(Q_k^{sp})}{V_k^4} + \frac{-P_{0k}V_{rk}^2(\beta_p + 2\gamma_p V_k) - Q_{0k}V_{rk}V_{mk}(\beta_q + 2\gamma_q V_k)}{V_k^3}$
	$J_2 = -B_{kk} - \frac{(Q_k^{sp})(V_{rk}^2 - V_{mk}^2) - 2V_{mk}V_{rk}(P_k^{sp})}{V_k^4} + \frac{-P_{0k}V_{rk}V_{mk}(\beta_p + 2\gamma_p V_k) - Q_{0k}V_{mk}^2(\beta_q + 2\gamma_q V_k)}{V_k^3}$
	$J_3 = B_{kk} - \frac{(Q_k^{sp})(V_{rk}^2 - V_{mk}^2) - 2V_{mk}V_{rk}(P_k^{sp})}{V_k^4} + \frac{-P_{0k}V_{mk}^2(\beta_p + 2\gamma_p V_k) + Q_{0k}V_{rk}V_{mk}(\beta_q + 2\gamma_q V_k)}{V_k^3}$
	$J_4 = G_{kk} - \frac{(P_k^{sp})(V_{rk}^2 - V_{mk}^2) + 2V_{rk}V_{mk}(Q_k^{sp})}{V_k^4} + \frac{-P_{0k}V_{mk}^2(\beta_p + 2\gamma_p V_k) + Q_{0k}V_{rk}V_{mk}(\beta_q + 2\gamma_q V_k)}{V_k^3}$
J_{pv-pv}	$J_1 = -B_{kk} - \frac{V_{mk}I_{rk}^{calc} - V_{rk}I_{mk}^{calc}}{V_k^2} - \frac{V_{mk}}{V_{rk}}\left(G_{kk} - \frac{P_k^{sp}}{V_k^2}\right)$
	$J_2 = -\frac{V_{mk}}{V_k^2}$
	$J_3 = G_{kk} + \frac{P_k^{sp}}{V_k^2} - \frac{V_{mk}}{V_{rk}}\left(B_{kk} - \frac{V_{mk}I_{rk}^{calc} - V_{rk}I_{mk}^{calc}}{V_k^2}\right)$
	$J_4 = \frac{V_{rk}}{V_k^2}$

Off-diagonal Elements			
J_{dr-dr}, J_{dr-pq},	$J1 = G_{km}$	J_{dr-pv}	$J1 = -B_{km} - \frac{V_{m,k}}{V_{r,k}}G_{km}$
J_{pq-dr}, J_{pq-pq},	$J2 = -B_{km}$	J_{pq-pv}	$J2 = 0$
J_{pv-dr}, J_{pv-pq},	$J3 = B_{km}$	J_{pv-pv}	$J3 = G_{km} - \frac{V_{m,k}}{V_{r,k}}B_{km}$
	$J4 = G_{km}$		$J4 = 0$

calculating the Jacobian Matrix in $(i+1)^{th}$ iteration, the real and imaginary part of bus voltages can be calculated by using following equation.

$$v^{i+1} = v^i + J^{-1}\triangle, \tag{4.21}$$

where

$$v = [V_r^T V_m^T]^T, \tag{4.22}$$

and V_r and V_m are the vectors of real and imaginary parts of voltages of all the system buses except the AR bus.

It is worth mentioning that the NR algorithm can be utilized to solve the PF of DCIMG as proposed in [2, 56, 99, 100] and [101]. For CINR to be able to solve the PF of islanded microgrid implemented with the droop control, few aspects need to be discussed. Firstly, the voltage magnitude of the AR bus is not fixed. Secondly, the system frequency is variable. To resolve these issues, this chapter introduces an iterative approach to update the system frequency and voltage magnitude of AR bus.

4.3.3 Update of the System Frequency and AR Bus Voltage

To determine the PF of DCIMG using CINR algorithm, AR bus is assumed as slack bus. So, the operating states (voltage magnitude) of the AR bus and system frequency must be fixed prior to applying the CINR for performing PF analysis. To address this issue, a loop of operations is proposed in this paper. The objective of this loop is to regulate the voltage of the AR bus and system frequency in order to satisfy the droop characteristics of DCIMG.

The proposed loop-based methodology is shown in figure 4.1 and following steps are performed to solve the PF problem of droop control based islanded microgrids using CINR.

1. At the first step, the initial operating condition is determined. In this step, one droop bus is selected as an AR bus. Variables ω_{grid} and V_s are initialized on their nominal value, ω_0 and $V_{0,s}$ respectively.

2. Afterward, calculate the bus admittance matrix at the system frequency ω_{grid}. In addition, the scheduled generation of active and reactive power at droop buses are calculated using equations (4.7) and (4.8)

3. In this step, PF analysis is done using the CINR algorithm. The main aim of this step is to determine the total injected real and reactive powers in all droop buses including AR bus. These injected real and reactive powers will be further used to update the system frequency and voltage magnitude at AR bus.

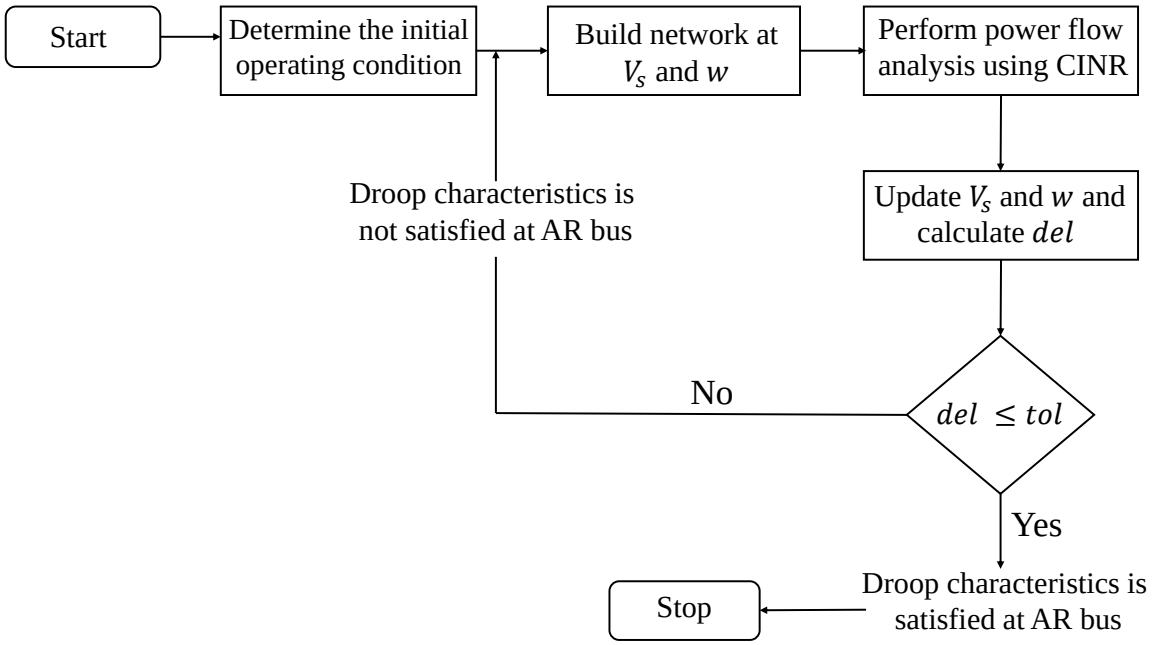

Figure 4.1: Flow chart of CINR

4. In this approach, the system frequency is updated using following equation.

$$w_{grid}^{i+1} = w_0 - \left(\sum_{k=1} \frac{1}{m_k(x_k P_{G,k} - y_k Q_{G,k})} \right)^{-1} \tag{4.23}$$

5. The magnitude of voltage at AR bus is updated as follows.

$$V_s^{i+1} = (1-\alpha)(V_s^i) + \alpha(|V_{0,s}| - n_s(y_s P_{G,s} + x_s Q_{G,s})) \tag{4.24}$$

6. After updating the system frequency and voltage magnitude of AR bus, a variable *del* is calculated using equation (4.25) to check the termination criteria.

$$del = max\{|w_{grid}^{i+1} - w_{grid}^{i}|, |V_s^{i+1} - V_s^i|\} \tag{4.25}$$

7. If the value of *del* is smaller than the pre-specified tolerance, the iterative loop is terminated and the previous PF results are selected as the final PF solution.

8. While, if the value of *del* is not smaller than tolerance, the next loop is performed with updated values and this procedure continues until the value of *del* becomes smaller than the tolerance.

Table 4.3: Data required for modeling of the six bus test system in time-domain

m_p (rad/s/W)	n_q (V/VAR)	w^* (rad/sec)	V^* (V)
$9.4E-05$	$1.3E-03$	377	127

Line parameters			
From bus	To bus	$R_{line}(\Omega)$	$L_{line}(mH)$
1	2	0.43	0.32
1	4	0.30	0.35
2	5	0.20	0.25
2	3	0.15	1.84
3	6	0.05	0.05

Load parameter		
bus number	$R_{load}(\Omega)$	$L_{load}(mH)$
1	6.95	12.20
3	5.01	9.40

4.3.4 Validation of CINR

To confirm the applicability and accuracy of the proposed power flow algorithm, the obtained results are compared with the time-domain model of a droop control based islanded microgrid. For algorithm validation, a six-bus test system (shown in Fig. (4.5)) is considered. The detailed time domain model of this system has been simulated in PSCAD/EMTDC, a time-domain simulation environment as discussed in [163] and [169]. The data used to model this system in time-domain is presented in Table-4.3 . This system has three droop control based DG which are working in an islanded mode.

To solve the power flow of this test system using CINR, the algorithm has been developed in MATLAB. The result obtained from PSCAD and CINR are depicted in Table-4.4. As shown in Table-4.4, the maximum errors in voltage magnitude and angle are 0.0081% and 0.26% respectively. This good agreement within the obtained results validates the accuracy of the CINR in solving the power flow of droop control based islanded MG. Moreover, PSCAD requires approximately 172s to attain the steady-state, while the CINR requires 0.04s.

Table 4.4: Validation of results obtained for six-bus test system.

Bus	Voltage magnitude (V)		Angle (rad)		Active Power (kw)		Reactive Power (kvr)	
	PSCAD	CINR	PSCAD	CINR	PSCAD	CINR	PSCAD	CINR
1	121.92	121.92	0.0078	0.0078	-0.0189	-0.0189	-0.0125	-0.0125
2	123.51	123.51	-0.0013	-0.0013	0	0.000	0	0.0000
3	122.42	122.42	-0.0388	-0.0389	-0.0253	-0.0253	-0.0179	-0.0179
4	125.37	125.37	0.0065	0.0065	0.0151	0.0151	0.0075	0.0075
5	125.74	125.74	0*	0*	0.0151	0.0151	0.0058	0.0058
6	123.11	123.10	-0.0420	-0.0421	0.0151	0.0151	0.0179	0.0179
err	0.0081%		0.26%		0.0005%		0.0003%	
freq	376.6645	376.6645						
Time	172s	0.04s						

4.3.5 Performance Analysis of CINR

Comparison of CINR with MNR and NTR

In this section, four radial (CASE6, CASE22, CASE38, and CASE69) and one meshed (CASE160) distribution systems are considered to compare the results obtained from CINR with the results obtained from MNR and NTR. The extensive data of these test systems are reported in Appendix-II. Four different cases including: 1) conventional droop, 2) inverse droop, 3) mixed droop, and 4) isochronous mode of operation are studied to demonstrate the robustness of the proposed algorithm for the different operating modes of droop-based DGs.

All the algorithms are executed on MATLAB R2017b in PC with an INTEL Core i7 @ 3.2 GHz, 8 GB of RAM. The flat start is considered as an initial solution in all algorithms (for operating frequency the flat start is 1.0 p.u.). The stopping criteria for all the algorithms are same and selected in a way that either the gradient norm or the total number of iterations does not exceed the specified value. The solutions for CASE22, CASE38, and CASE69 including bus powers have been given in appendix IV.

It is to be noted that the NTR algorithm is implemented only for case 1 and MNR is not implemented for case 4 (isochronous operation). Therefore, the power flow results for these cases are not available. For case 1 (conventional droop), all the algorithms are applicable and the power flow results obtained from the algorithms are similar except MNR which fails to provide a solution in case of CASE69 and CASE160. Similarly, in cases 2, 3, and 4, CINR and MNR provide similar power flow results for CASE22, and CASE38 but MNR fails to provide a solution for CASE69 and CASE160. For case 5, only

Table 4.5: Computation time required to solve power flow for different cases considering CINR, MNR and NTR algorithm. (NC: Not Converged, NA: Not Applicable, CT: Computation Time, %: Percentage improvement in computation time.)

System	Cases	CINR	MNR		NTR	
		CT(s)	CT(s)	%	CT(s)	%
CASE22	1	4.96E-03	6.35E-02	1180.16	1.77E-02	256.63
	2	5.58E-03	4.84E-02	767.82	NA	NA
	3	4.22E-03	4.98E-02	1080.50	NA	NA
	4	3.81E-03	NA	NA	NA	NA
CASE38	1	2.22E-02	1.46E-01	556.68	3.48E-02	56.83
	2	1.42E-02	1.59E-01	1020.27	NA	NA
	3	2.28E-02	1.64E-01	621.31	NA	NA
	4	2.36E-02	NA	NA	NA	NA
CASE69	1	1.33E-02	NC	NC	1.43E-01	970.79
	2	1.72E-02	NC	NC	NA	NA
	3	1.82E-02	NC	NC	NA	NA
	4	1.81E-02	NA	NA	NA	NA
CASE160	1	6.08E-02	NC	NC	5.10E-01	738.64
	2	4.99E-02	NC	NC	NA	NA
	3	4.47E-02	NC	NC	NA	NA
	4	6.03E-02	NA	NA	NA	NA

CINR can provide the power flow solutions because MNR and NTR are not defined for an isochronous mode of operation.

To analyze the performance of MNR, NTR, and CINR in terms of computation time, the time required to obtain the power flow solution is recorded for all the cases and reported in Table 4.9. It is found that expected execution time for the cases CASE22 and CASE38, CINR is almost 10 times faster than MNR. Similarly, CINR is approximately 3, 2, and 9 times faster than NTR for the cases CASE22, CASE38, and CASE69, respectively.

From the above analysis, it can be concluded that the solutions obtained by CINR converges faster in comparison to MNR and NTR without compromising the accuracy. Additionally, CINR can also be used to perform power flow analysis for the systems

having DGs with several types of droop characteristics including the isochronous mode of operation.

Robustness of CINR

The performance of power flow algorithms depends on the r/x ratio of lines and the loading condition of the system. Hence, it is also desired to investigate the robustness of the proposed algorithm for different system loading conditions and various r/x ratio of lines. The CASE38 is considered for the study which has a radial structure with lines having a high r/x ratio and zone wise voltage dependent loads. The performance of CINR, MNR, and NTR in terms of computation time for different r/x ratios of line and system loading condition is shown in Figures (4.2) and (4.3) respectively. It is clear from Figures (4.2) and (4.3) that the CINR requires less computation time to obtain the power flow solution of CASE38 for different cases, while MNR requires more computation time as MNR is not designed to deal with the voltage dependent loads.

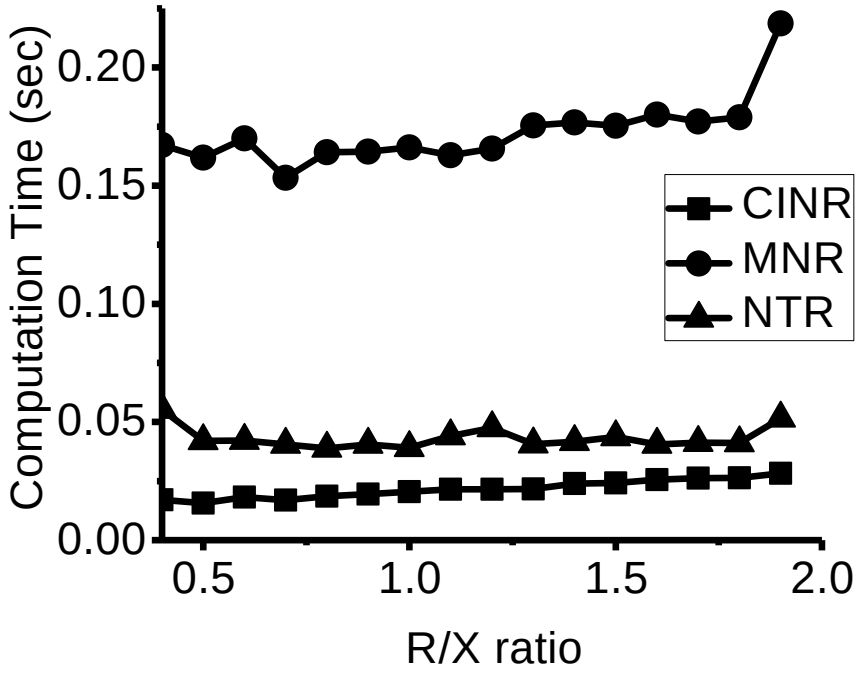

Figure 4.2: r/x ratio vs computation time (sec) for CASE38 test systems.

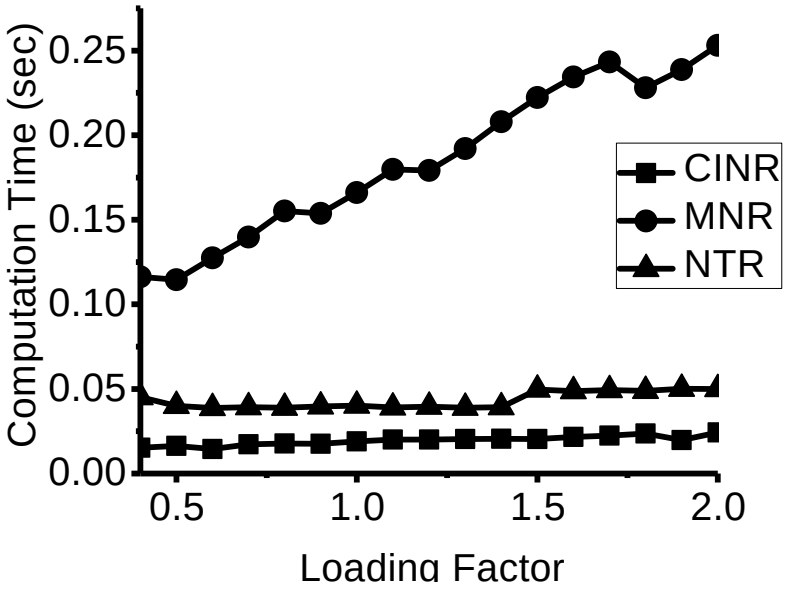

Figure 4.3: Loading factor vs computation time (sec) for CASE38 test systems.

4.4 Nested Backward/Forward Sweep Algorithm for DCIMG

In this section, the main steps of the NBFS algorithm is discussed in detailed. The proposed algorithm is divided into three steps: modified backward sweep, modified forward sweep, and system frequency & reference voltage update. To calculate the initial value of the power flow variables, initialization of parameters including system frequency and node voltages are required. Initialization, modified backward sweep, modified forward sweep and the system frequency & reference voltage update procedure are as follows:

4.4.1 Initialization

The first step of initialization is to select one of the droop buses as a AR bus. Then, the system frequency and voltage of every bus are initialized at 1 pu. Tolerance value for both (voltage and frequency) loops are set to 10^{-8}.

4.4.2 Modified Backward Sweep

The backward sweep is the first sweep applied in conventional BFS algorithm. In this sweep, the branch current is calculated based on the assumption that the voltage of all

the buses are known. Therefore, the branch currents are calculated using the apparent power injected to the buses and the bus voltages. In the case of PQ buses, the apparent injected power is calculated as:

$$S_i = P_i + jQ_i = (P_{g,i} - P_{l,i}) + j(Q_{g,i} - Q_{l,i}) \tag{4.26}$$

Since, in the case of droop buses, the generation depends on the bus voltage and the system frequency. To calculate the apparent power at each droop buses equation (4.27) is formulated using equations (4.7), (4.8), and (4.26) which is given as:

$$\begin{aligned} S_i = (P^o_{g,i} + m_{P,i}(w_o - w) - P_{l,i}) + j(Q^o_{g,i} + n_{Q,i}(|V_o| - \\ |V_i|) - Q_{l,i}) \end{aligned} \tag{4.27}$$

The apparent power (calculated as per equation 4.27) is applied to calculate the bus current which is as follows:

$$I_i = \left(\frac{S_i}{V_i}\right)^* \tag{4.28}$$

These bus currents (equation 4.28) are summed in the backward direction from the farthest buses towards the reference bus to calculate the branch currents and this procedure is described using the following equation:

$$[\mathbf{I}_{ij}] = [\mathbf{BIBC}][\mathbf{I}_i] \tag{4.29}$$

where, the transformation matrix **BIBC** is defined in subsection 4.4.4.

4.4.3 Modified Forward Sweep

In conventional algorithm, the forward sweep is applied to update the bus voltages using the calculated branch current of the backward sweep. This step includes the calculation of voltages from the AR bus to lower stream buses using branch impedances and branch currents. In other words, the bus voltages can be also calculated using the reference voltage, branch impedance, and branch current which is represented as:

$$[\mathbf{V}] = [\mathbf{V}_{ref}] - [\mathbf{BCBV}][\mathbf{I}_{ij}] \tag{4.30}$$

where, the transformation matrix BCBV is used to calculate voltages using branch currents and the computation of this matrix is described in detail in subsection 4.4.4. $[\mathbf{V}_{ref}]$ and $[\mathbf{V}]$ represent the voltage of AR bus and rest other buses in the system respectively.

As we know that in the conventional droop control technique, reactive power sharing among the sources are not proportional as per their rating. Due to disproportional reactive power sharing among the sources, there may be a chance that the obtained current reaches very high value in some cases. This may cause a larger deviation in voltage from the operating point. This larger deviation in voltage may diverge the solution. To overcome this issue, a decelerating factor (β) in the voltage update equation is proposed in this paper which is given in equation (4.31).

$$[\mathbf{V}]^{k+1} = (1-\beta)[\mathbf{V}]^{k} + \beta([\mathbf{V}_{ref}] - [\mathbf{BCBV}][\mathbf{I}_{ij}]) \tag{4.31}$$

where, the value of β must be in range of 0 to 1. The role of β is to adjust the length of voltage correction vector ($[\triangle\mathbf{V}]^{k+1} = [\mathbf{V}]^{k} - [\mathbf{V}_{ref}] + [\mathbf{BCBV}][\mathbf{I}_{ij}]$) to overcome the larger deviation in the voltage correction vector. In the manuscript, the value of β is set to 0.5 for all the cases. It is to be noted that the value β is not optimal at 0.5 for every test system. Although, it performs very well on a wide range of problems.

4.4.4 Calculation of BIBC and BCBV

The first step is to calculate the node incidence matrix, A. Upon calculation of A, the matrices **BIBC** and **BCBV** are calculated. The size of matrix A is $(N_b \times N)$ where, N_b and N indicate the number of branches and nodes of the system respectively. The $(i\text{-}j)^{th}$ element of A, a_{ij}, is:

1. $a_{ij} = +1$ when current leaves the node j from branch i
2. $a_{ij} = -1$ when current flows towards the node j from branch i
3. $a_{ij} = 0$ when there is no connection between the node j and branch i

According to the network theory, branch and node currents are associated as:

$$[\mathbf{I}_i] = A^t[\mathbf{I}_{ij}] \tag{4.32}$$

where, $[\mathbf{I}_i]$ and $[\mathbf{I}_{ij}]$ represent the node and branch current vectors respectively and superscript t indicates the transpose of the matrix.

However, in the backward sweep, the branch currents are required to calculate from the bus injected currents. Therefore, from equation (4.32).

$$[\mathbf{I}_{ij}] = (A^t)^{-1}[\mathbf{I}_i] \tag{4.33}$$

where $(\ldots)^{-1}$ indicates the inverse of a matrix.

In general, $N_b \neq N$, so the matrix A is non-invertible. However, in the case of a radial system ($N_b = N - 1$), by eliminating the first column from A, corresponding to AR bus, the branch currents can be directly computed from the node currents. It may be noted that the first column of A (corresponding reference node) can be eliminated because this node is not a participant of the backward process of BFS.

After comparing the equations (4.29) and (4.33), the specific procedure to build **BIBC** on the basis of network theory indicates that $\mathbf{BIBC} = (A^t)^{-1}$.

For the special case of a square incidence matrix A graph theory shows that:

$$[\mathbf{V}_i] = (A)^{-1}[\mathbf{V}_{ij}] \tag{4.34}$$

where, $[\mathbf{V}_i]$ and $\mathbf{V}_{ij}$ indicate the node and branch voltage vector respectively.

$[\mathbf{V}_{ij}]$ can be obtained as:

$$[\mathbf{V}_{ij}] = diag([\mathbf{Z}_{ij}])[\mathbf{I}_{ij}] \tag{4.35}$$

where, $diag([\mathbf{Z}_{ij}])$ indicates the diagonal matrix of the branch impedances. Accordingly, the bus voltages in the forward sweep is calculated as:

$$[\mathbf{V}_i] = [\mathbf{V}_{ref}] - (A)^{-1} diag([\mathbf{Z}_{ij}])[\mathbf{I}_{ij}] \tag{4.36}$$

From equations (4.30) and (4.36), it can be found that $\mathbf{BCBV} = (A)^{-1} diag([\mathbf{Z}_{ij}])$. The detailed description about the formation of the matrices **BIBC** and **BCBV** can be found in [36-37].

4.4.5 Frequency and AR Bus Voltage Update

This step is basically a correction step of system frequency and the reference voltage. The system frequency and voltage of AR bus is a global variable in the case of DCIMGs. Therefore, these values must be adjusted after each iteration until the convergence is reached. The AR bus is also the droop bus but it behaves like the upstream bus. Hence, the droop characteristics of AR bus is also satisfied at the equilibrium state. Based on the mismatch of droop characteristics of AR bus, the value of system frequency and voltage of AR bus is updated. In droop controlled MGs, the system frequency depends on the total active power-sharing of the DGs, where all the DGs behave as a single source with

equivalent frequency droop . The equivalent droop ($m_{P,equ}$) of the system is calculated as:

$$m_{P,equ} = \frac{1}{\sum_{k\epsilon DB} \frac{1}{m_{P,k}}}$$

where, DB is a set of all droop buses and $m_{P,k}$ is a droop coefficient corresponding to $P-\omega$ droop for k^{th} bus. The new system frequency is obtained as:

$$w^{m+1} = w_o - \frac{1}{m_{P,equ}} \left(\sum_{k\epsilon DB} (P^o_{g,k} - P^{m+1}_{g,k}) \right) \tag{4.37}$$

where, m indicates the loop index.

The change in system frequency causes the change in the line reactance which is modified as:

$$X^{m+1}_{ij} = w^{m+1} L_{ij} \tag{4.38}$$

In addition, the net imbalance of voltage droop, $\triangle V$, at the AR bus is used to update the voltage of the AR bus. The $\triangle V$ is calculated using equation (4.39) and the voltage of AR bus is updated using equation (4.40).

$$\triangle V^{m+1} = (V_o - |V_{AR}|^m) + \frac{1}{n_{Q,AR}} \left(Q^o_{g,AR} - Q^{m+1}_{g,AR} \right) \tag{4.39}$$

$$V^{m+1}_{ref} = V^m_{ref} + \alpha \triangle V^{m+1} \tag{4.40}$$

where, V_o is a nominal voltage of AR bus and α is declaration factor whose value lies between 0.3 to 1.5. The flow chart of the proposed algorithm is shown in Fig. (4.4).

4.4.6 Validation of NBFS

In this section, the proposed algorithm NBFS is validated on a small 6-bus test system (Fig. 4.5). Details of the system including droop parameters, line and load data, rated voltage and system frequency is given in Table 4.3. To illustrate its effectiveness and accuracy, the result obtained from the proposed algorithm is compared with the result obtained from the time-domain model of the test system. The NBFS is implemented to obtain the load flow solution of the network. The time-domain model of the test system is simulated in the PSCAD/EMTDC and results are presented in Table 4.6.

The result shows that the NBFS provides a similar corresponding value of voltage and angle in comparison to the solution obtained from PSCAD/EMTDC which shows the

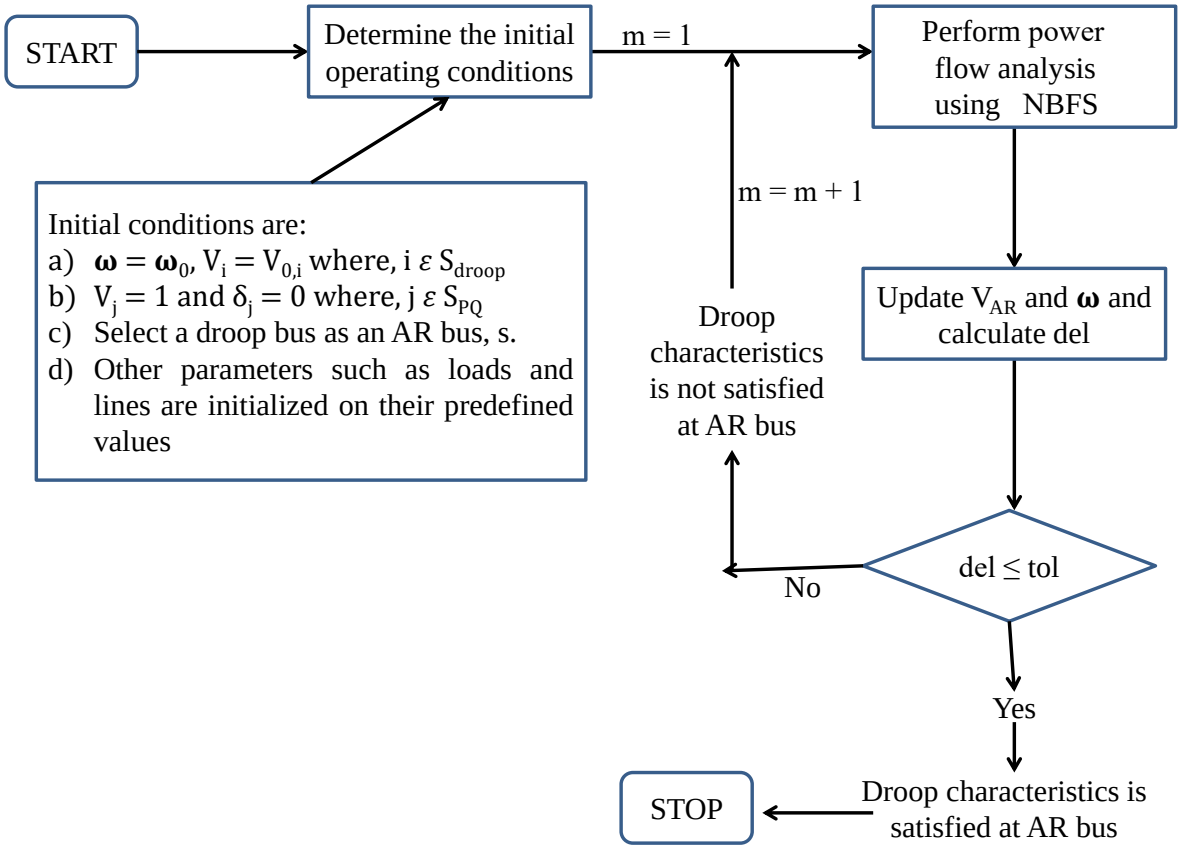

Figure 4.4: Flow chart of NBFS

accuracy of the proposed algorithm. It is to be noted that to achieve the converged solution, NBFS takes execution time approximately 0.008 sec which is very less as compared to the required simulation time of PSCAD.

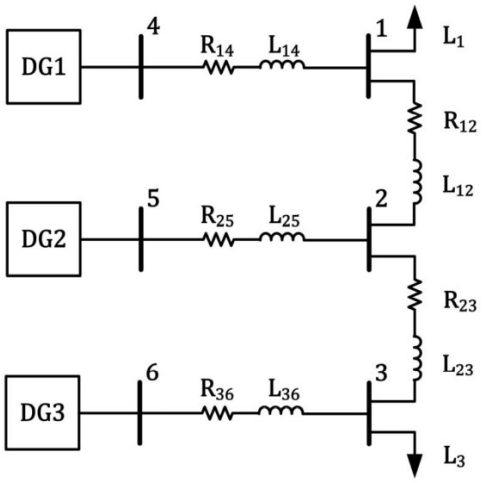

Figure 4.5: 6-bus MG [2].

Table 4.6: Validation of obtained result of the six-bus test system

Bus	Voltage magnitude (V)		Angle (rad)	
	PSCAD	NBSF	PSCAD	NBSF
1	121.92	121.92	0.0078	0.0078
2	123.51	123.51	-0.0013	-0.0013
3	122.42	122.42	-0.0388	-0.0389
4	125.37	125.37	0.0065	0.0065
5	125.74	125.74	0*	0*
6	123.11	123.10	-0.0420	-0.0421
err	0.0081%		0.26%	
freq	376.6645	376.6645		
Time	172s	0.009s		

4.4.7 Performance Analysis of NBFS

Comparison of NBFS with DBFS and MBFS

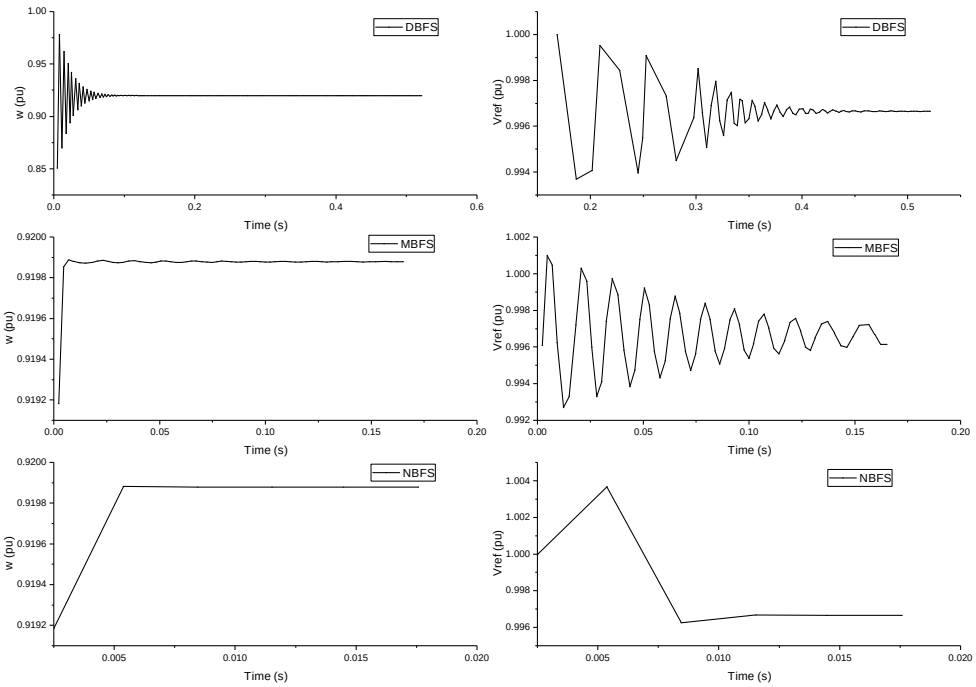

Figure 4.6: Convergence of the solution with respect to computation time for CASE33 system

In this section, a detailed comparison among the load flow solutions (obtained for droop based islanded microgrid) applying NBFS, DBFS, and MBFS are presented.

CASE33 radial distribution test system is adopted to compare result of the proposed algorithm with the DBFS [98] and MBFS [174]. The droop parameter and test settings are directly adopted from [174] and [98] for fair comparison. Additionally, results of PSCAD/EMTDC are also included for validation. Table 4.7 shows the results given

Table 4.7: NBFS algorithm versus DBFS, MBFS, and PSCAD/EMTDC results for CASE33 system. (1* represents the AR bus)

Bus	Voltage Magnitude (pu)				Active Load (pu)				Reactive Load (pu)			
	DBFS	MBFS	PSCAD	NBFS	DBFS	MBFS	PSCAD	NBFS	DBFS	MBFS	PSCAD	NBFS
1*	0.996	0.997	0.997	0.997	0.00	0.00	0.00	0.00	0.00	0.00	0.00	0.00
2	0.996	0.996	0.996	0.996	0.20	0.20	0.20	0.20	0.12	0.12	0.12	0.12
3	0.993	0.993	0.993	0.993	0.18	0.18	0.18	0.18	0.08	0.08	0.08	0.08
4	0.992	0.992	0.992	0.992	0.24	0.24	0.24	0.24	0.16	0.16	0.16	0.16
5	0.991	0.992	0.992	0.992	0.12	0.12	0.12	0.12	0.06	0.06	0.06	0.06
6	0.991	0.991	0.991	0.991	0.12	0.12	0.12	0.12	0.04	0.04	0.04	0.04
7	0.990	0.990	0.990	0.990	0.40	0.40	0.40	0.40	0.20	0.20	0.20	0.20
8	0.990	0.990	0.990	0.990	0.40	0.40	0.40	0.40	0.20	0.20	0.20	0.20
9	0.992	0.992	0.992	0.992	0.12	0.12	0.12	0.12	0.04	0.04	0.04	0.04
10	0.994	0.994	0.994	0.994	0.12	0.12	0.12	0.12	0.04	0.04	0.04	0.04
11	0.995	0.995	0.995	0.995	0.09	0.09	0.09	0.09	0.06	0.06	0.06	0.06
12	0.996	0.995	0.995	0.995	0.12	0.12	0.12	0.12	0.07	0.07	0.07	0.07
13	1.001	1.001	1.001	1.001	0.12	0.12	0.12	0.12	0.07	0.07	0.07	0.07
14	0.999	0.999	0.999	0.999	0.24	0.24	0.24	0.24	0.16	0.16	0.16	0.16
15	0.998	0.997	0.997	0.997	0.12	0.12	0.12	0.12	0.02	0.02	0.02	0.02
16	0.997	0.996	0.996	0.996	0.12	0.12	0.12	0.12	0.04	0.04	0.04	0.04
17	0.995	0.994	0.994	0.994	0.12	0.12	0.12	0.12	0.04	0.04	0.04	0.04
18	0.994	0.994	0.994	0.994	0.18	0.18	0.18	0.18	0.08	0.08	0.08	0.08
19	0.995	0.995	0.995	0.995	0.18	0.18	0.18	0.18	0.08	0.08	0.08	0.08
20	0.992	0.992	0.992	0.992	0.18	0.18	0.18	0.18	0.08	0.08	0.08	0.08
21	0.991	0.991	0.991	0.991	0.18	0.18	0.18	0.18	0.08	0.08	0.08	0.08
22	0.990	0.991	0.990	0.990	0.18	0.18	0.18	0.18	0.08	0.08	0.08	0.08
23	0.992	0.992	0.992	0.992	0.18	0.18	0.18	0.18	0.10	0.10	0.10	0.10
24	0.990	0.990	0.990	0.990	0.84	0.84	0.84	0.84	0.40	0.40	0.40	0.40
25	0.991	0.991	0.991	0.991	0.84	0.84	0.84	0.84	0.40	0.40	0.40	0.40
26	0.990	0.990	0.990	0.990	0.12	0.12	0.12	0.12	0.05	0.05	0.05	0.05
27	0.989	0.990	0.989	0.989	0.12	0.12	0.12	0.12	0.05	0.05	0.05	0.05
28	0.985	0.986	0.986	0.986	0.12	0.12	0.12	0.12	0.04	0.04	0.04	0.04
29	0.983	0.984	0.984	0.984	0.24	0.24	0.24	0.24	0.14	0.14	0.14	0.14
30	0.983	0.984	0.983	0.983	0.40	0.40	0.40	0.40	1.20	1.20	1.20	1.20
31	0.985	0.986	0.986	0.986	0.30	0.30	0.30	0.30	0.14	0.14	0.14	0.14
32	0.987	0.988	0.988	0.988	0.42	0.42	0.42	0.42	0.20	0.20	0.20	0.20
33	0.990	0.990	0.990	0.990	0.12	0.12	0.12	0.12	0.08	0.08	0.08	0.08
Max Error	0.001	0.001	–	0.000	0.00	0.00	–	0.00	0.00	0.00	–	0.00
					Active Generation (pu)				Reactive Generation (pu)			
1	0.996	0.997	0.997	0.997	2.494	2.502	2.502	2.502	0.978	0.967	0.967	0.967
6	0.991	0.991	0.991	0.991	0.981	0.980	0.980	0.980	0.904	0.909	0.909	0.909
13	1.001	1.001	1.000	1.000	1.707	1.701	1.701	1.701	0.931	0.893	0.893	0.893
25	0.991	0.991	0.991	0.991	0.981	0.980	0.980	0.980	0.904	0.909	0.909	0.909
33	0.990	0.990	0.990	0.990	1.304	1.301	1.301	1.300	0.916	0.948	0.948	0.948
Max Error	0.001	0.001		0.000	0.008	0.000		0.000	0.038	0.000	0.000	0.000
					Pg	Qg	Pl	Ql	Ploss	Qloss	freq	CT(s)
				DBFS	7.467	4.633	7.430	4.600	0.037	0.033	0.919	0.521
				MBFS	7.464	4.626	7.430	4.600	0.034	0.026	0.920	0.165
				PSCAD	7.463	4.625	7.430	4.600	0.035	0.027	0.920	462.142
				NBFS	7.463	4.626	7.430	4.600	0.035	0.026	0.920	0.018

in [98] and [174] in addition to the results obtained from NBFS and PSCAD/EMTDC.

For a fair comparison, the nominal power of all DGs is set at $0.9 + j0.9$ pu and bus 1 is considered as the AR bus. Therefore, the power reported in Table 4.7 is an apparent power which is the sum of nominal power and the power generated due to drop in frequency and voltage. It is clearly seen from Table 4.7, the obtained system frequency is similar for all the algorithms, while there is some difference in the magnitude of bus voltages. The maximum mismatch of voltage magnitude, real power, and reactive power are also reported in Table 4.7. This maximum mismatch is calculated after considering the result of PSCAD/EMTDC as a standard solution of PF problem. From Table 4.7, it can say that the solution of NBFS is nearer to the solution of PSCAD/EMTDC as compared to other solutions obtained with application of other algorithms. Hence, the obtained solution of NBFS is more accurate than the solution of MBFS and NBFS.

In DBFS, the obtained reactive power generation of DGs is slightly different from the result obtained from MBFS and NBFS. DBFS uses an inner and outer loop update schemes in such a way that the voltage of DG is updated in the inner loop using BFS while the voltage magnitude of reference bus remains constant [98]. When the inner loop converges, the voltage magnitude of AR bus is updated based on the reactive power mismatch and the voltages of other buses according to the droop law. On the other hand, MBFS and NBFS are governed by the droop law of the DGs, so their output reactive power are closer to the results obtained in the time domain simulation in PSCAD/EMTDC.

To further analyze difference between the performance of NBFS, MBFS, and DBFS; the dynamics of system frequency and voltage magnitude of AR bus (Bus 1) with respect to time is depicted in Fig 4.6. It is clearly seen from Fig. 4.6 that in comparison to MBFS and DBFS, the required computation time is very less in NBFS to achieve the converged power flow solution. The main reason behind this difference in computation time and dynamics is the variations in the basic structure of the algorithms. In NBFS, there is one loop where the system frequency and voltage magnitude of reference bus are updated to satisfy the droop characteristics of DG connected to the reference bus. For the other DGs, the generated power is updated in backward sweep step of BFS according to their droop characteristics. This structure of NBFS reduces the computational burden and increases the convergence speed as compared to MBFS and NBFS. Since the generated power of all the droop controlled DGs are updated outside the loop of BFS in MBFS and DBFS, in DBFS, different loops are utilized to update the real and reactive power separately which

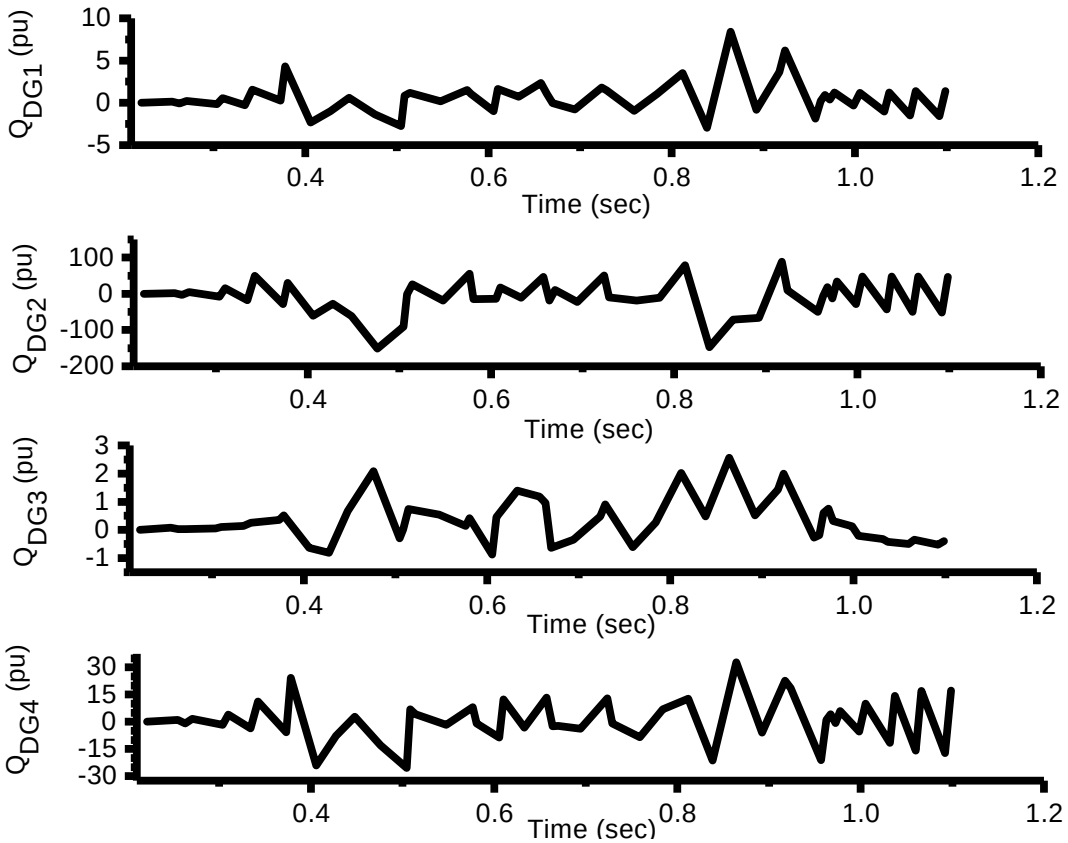

Figure 4.7: Divergence of MBFS for 33-bus test system

increases the computation burden which ultimately increases the convergence time to achieve the solution. It can be seen in the Fig. 4.6 that the deviation in system frequency and voltage magnitude of reference bus before the convergence is higher in DBFS while in the case of NBFS deviation is very less. This oscillatory behavior of MBFS and DBFS delays the convergence and also makes the algorithm unstable for hard PF problems. According to the discussed points, we can say that the efficiency and robustness of NBFS is better than the MBFS and DBFS.

Comparison of NBFS with NTR and MNR

In this section, to examine the robustness of the proposed algorithm to achieve the power flow solution, a comparative study among the proposed algorithm and Jacobian based algorithms (NTR and MNR) is performed.

Three test systems including CASE22, CASE38, and CASE69 are chosen to analyze the performance of DBFS, MBFS, NTR, MNR, and NBFS. The data for the droop controlled DGs are given in Table 4.8. The convergence time to achieve the PF solution for

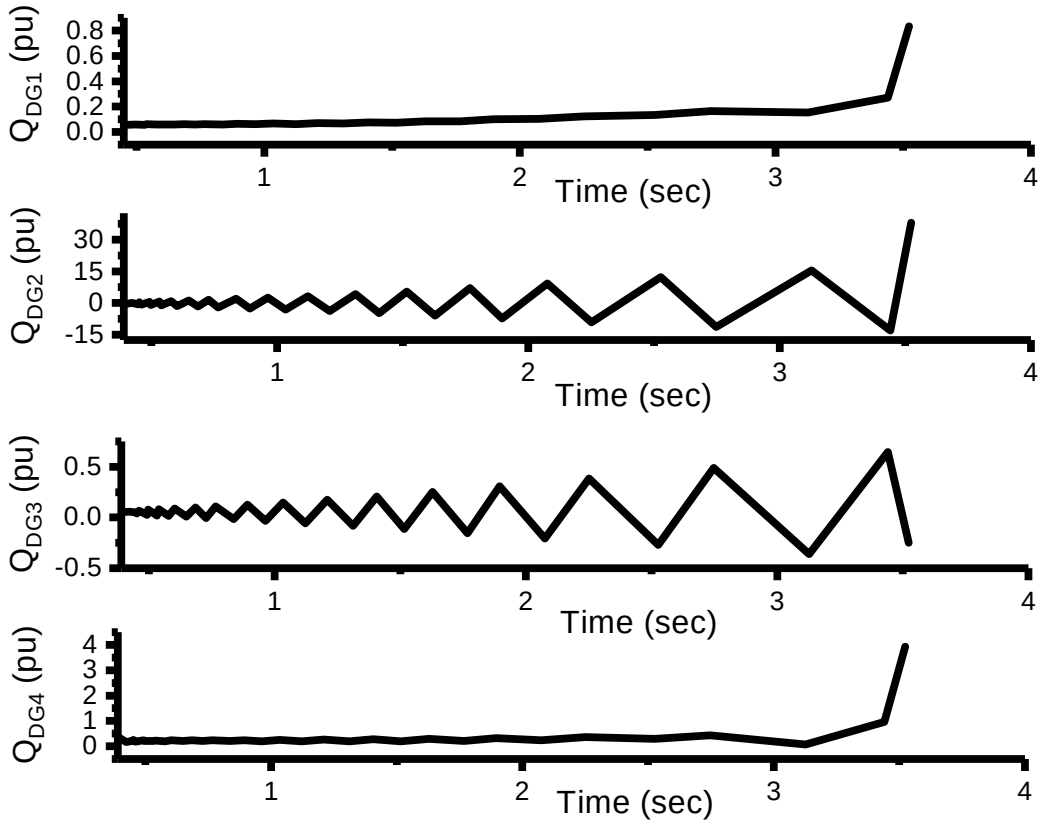

Figure 4.8: Divergence of DBFS for 33-bus test system

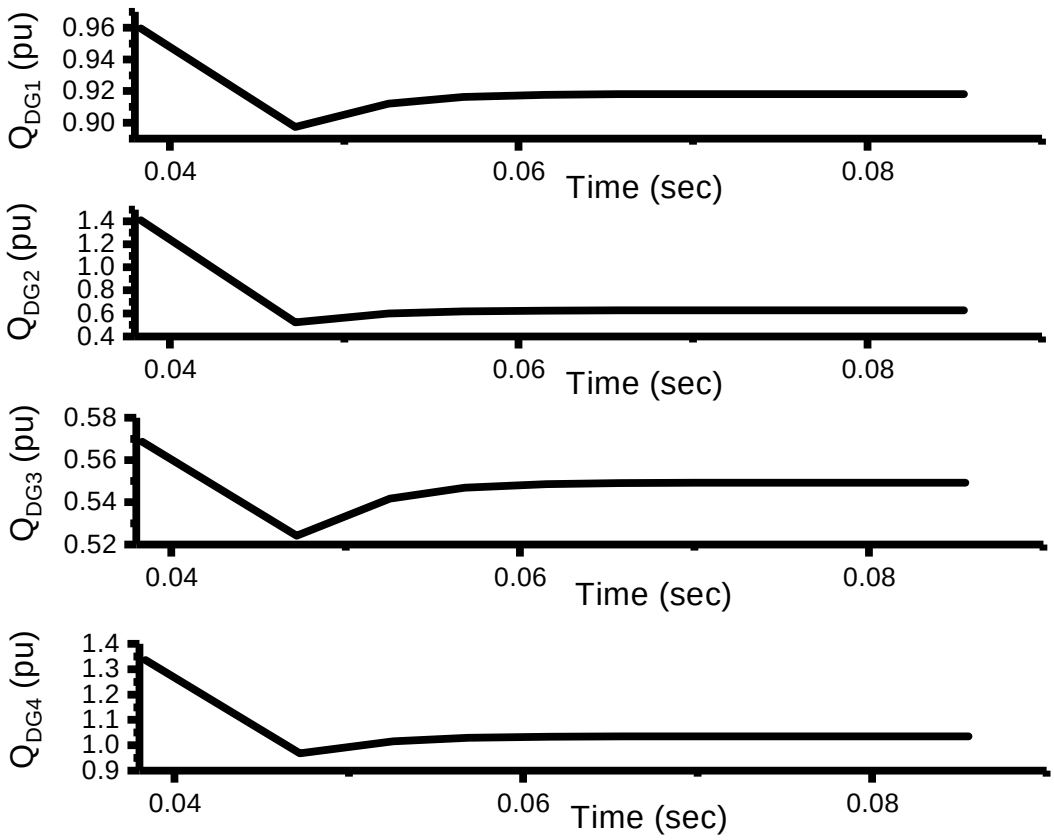

Figure 4.9: Convergence of NBFS for 33-bus test system

Table 4.8: Droop gains, nominal values and operative mode of DGs and Q_{max} limit for the 22-bus, 38-bus, and 69-bus test system.

Test System	Bus Number	m	n	w_0	$\|V_0\|$	Q_{max}
22-bus	5	0.005102	0.05	1	1	0.2
	13	0.001502	0.03	1	1	0.3
	15	0.004506	0.01	1	1	0.4
	21	0.001502	0.02	1	1	0.4
38-bus	34	0.005102	0.02	1	1.01	0.9
	35	0.001502	0.03333	1	1.01	0.6
	36	0.004506	0.02	1	1.01	0.9
	37	0.002253	0.05	1	1.01	0.3
	38	0.002253	0.05	1	1.01	0.3
69-bus	1	0.005102	0.05	1	1.01	0.35
	25	0.004506	0.05	1	1.01	0.45
	29	0.002253	0.01	1	1.01	0.9
	50	0.002253	0.1	1	1.01	0.6
	60	0.005102	0.1	1	1.01	1.5
	65	0.001502	0.03	1	1.01	0.9

Table 4.9: Computation time (in second) required to solve power flow for 22-bus, 38-bus, and 69-bus systems considering NBFS, MNR, NTR, MBFS, and NBFS algorithm. (NC: Not Converged)

System	NBFS	MNR	NTR	MBFS	DBFS
22-bus	4.96E-03	6.35E-02	1.77E-02	NC	NC
38-bus	3.01E-02	1.46E-01	3.48E-02	NC	NC
69-bus	4.33E-02	NC	1.43E-01	NC	NC

all the three systems are obtained for each algorithm (MBFS, DBFS, MNR, NTR, and NBFS) which are given in Table 4.9. It is clearly seen from the Table 5 that the MBFS and DBFS did not converge on a single test system due to their dynamics characteristic which is discussed in the previous section. In all test systems, the required time to

converge is lesser in case of NBFS as compared to MNR and NTR because:

- NBFS does not require calculation of the Jacobian matrix to achieve the PF solution.
- In MNR and NTR, bus admittance matrix is calculated at every iteration due to change in frequency, while NBFS does not require bus admittance matrix.
- In the case of MNR, CASE69 system does not reach convergence because MNR operates at the boundary of the solvable and unsolvable region in this case.

Discussion

The performance of the proposed algorithm NBFS is compared fairly with the performance of algorithms MBFS, DBFS, MNR, and NTR on three test system. It is found that among three test system, the MBFS and DBFS achieve the PF solution for only one test system. Hence, the performance of NBFS is only analyzed for the CASE33 test system in comparison with MBFS and DBFS and it is found that the NBFS is more efficient and robust than the MBFS and NBFS.

It is already discussed that the main reason behind the diversion of MBFS and DBFS is the oscillatory dynamics of system frequency and voltage magnitude of the reference bus. To show this behavior, MBFS and DBFS are applied on a CASE33 radial test system with droop parameter $\{0.005, 0.1, 0.01, 0.1, 0.02\}$. The resultant dynamics of reactive power generation of droop based DGs are shown in Figs. 4.7, 4.8 and 4.9 for MBFS, DBFS and NBFS respectively. It is clearly seen from the Figs. 4.7 and 4.8 that the generated reactive power of all droop controlled DGs are increased beyond the limit of the solvable region which leads the divergence in case of MBFS and DBFS. On the other hand, NBFS uses the deceleration factors α and β which behaves as a damper to the oscillation of system variables. This is the main reason behind the convergence of the NBFS algorithm in case of hard problems.

Both the MNR and NTR algorithms are Jacobian-based algorithm, in which the admittance matrix is also calculated to achieve the solution. The inverse of Jacobian Matrix is computationally bulky and increases with the increase of the size of the system. The effect of this computational burden is also shown in Table 4.9 where computation time for the convergence increases with the increase of the size of the system. Besides inverse of a Jacobian matrix, calculation of admittance matrix at every iteration also increases

the computational burden and complexity. In NBFS, these complex calculations are not required, so the algorithm requires less time to converge as compared to Jacobian based algorithms. Additionally, the system size does not affect the computation time much in the case of NBFS which is also seen from Table 4.9.

Performance of NBFS on weakly meshed islanded microgrid

In this sub-section, to show the robustness of the proposed algorithm for achieving the power flow solution of weakly meshed islanded microgrids, a comparative study among the algorithms NBFS, NTR, and MNR has been performed.

Table 4.10: The computation time (in second) required to solve power flow problem of CASE160 test system for NBFS, MNR, and NTR

System	NBFS	MNR	NTR
CASE160	6.08E-02	8.36E-01	5.10E-01

A 160-bus test system is selected to analyze the performance of NBFS, NTR, and MNR. The system data of this test system is adapted from [175]. In NBFS, the calculation procedure of matrices BIBC and BCBV are modified for weakly-meshed islanded system. The convergence time required to achieve the solutions are obtained for each algorithm (NBFS, NTR, and MNR) and are reported in Table 4.10. It is clearly seen from the Table 4.10 that the NBFS requires least time to converge in comparison to the MNR and NTR.

Comparison with conventional BFS on grid-connected microgrid

In this section, to examine the robustness of the proposed step of BFS of NBFS (pBFS) algorithm to achieve the PF solution of grid-connected microgrid, a comparative study between pBFS and conventional BFS (cBFS) algorithm is performed.

The CASE38 test system is selected to analyze the performance of pBFS and cBFS. The line and load data of the test system are adapted from [176]. System loads are increased from its base value (reported in [176]) by a different factor (λ) to analyze the robustness of the proposed pBFS algorithm in comparison to cBFS. The number of iterations and convergence time required to achieve the PF solution for the test system under different loading conditions is obtained for both the algorithms (pBFS and cBFS)

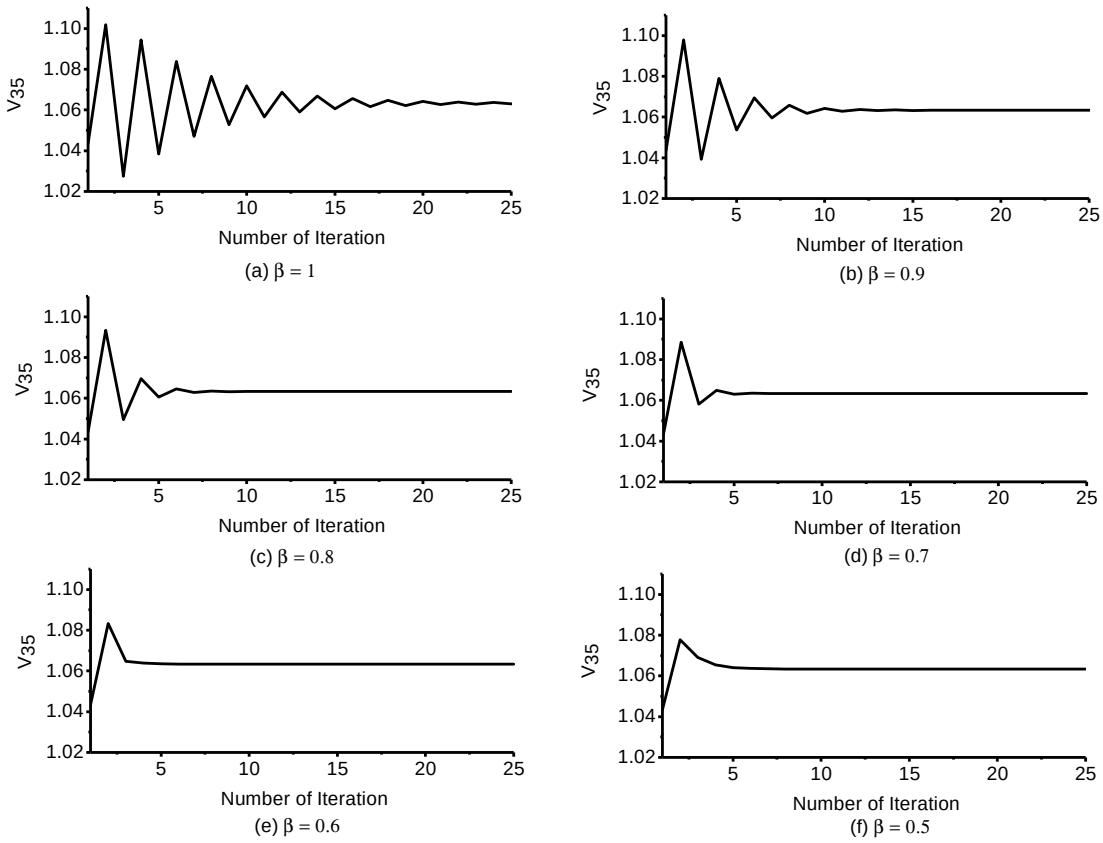

Figure 4.10: Effect of the value of β on the convergence of voltage magnitude of bus 35 of CASE38 test system in the case of $\lambda = 4$.

which are given in Table 4.11. It is clearly seen from Table 4.11 that the pBFS requires less number of iteration and less convergence time in comparison to cBFS for every loading condition. In addition, cBFS did not converge for the cases when $\lambda > 3$ due to the large variations of bus voltages in the initial iterations, while pBFS successfully converge for all the cases because the modified forward sweep uses a decelerating factor β to overcome the issue of the large variation in bus voltages in the initial few iterations. In the next subsection, the role of the parameter β is discussed.

Significance of the parameter β

The robustness of the proposed pBFS (step of NBFS) is highly improved as compared to the cBFS (conventional BFS) due to the parameter β which is used in equation (4.31) of the modified forward sweep. It is to be noted that the pBFS is reduced to cBFS for the value of $\beta = 1$. In this subsection, we have discussed the impact of β on the convergence behavior of the pBFS.

Table 4.11: Number of iteration and computation time (in second) required to solve power flow problem of CASE38 test system for different value of λ considering pB-FS and cBFS. (fail: fail to supply solution within 50 iteration, NC: Not Converged, NA: Not Available, It: Number of iteration, CT: Computation Time (in second))

λ	pBFS		cBFS	
	It	CT	It	CT
1.0	8	3.24E-03	11	4.72E-03
1.5	10	4.02E-03	15	7.03E-03
2.0	12	4.72E-03	20	8.12E-03
2.5	13	5.01E-03	26	1.12E-02
3.0	15	6.01E-03	35	1.52E-02
3.5	17	6.24E-03	fail	NA
4.0	19	7.35E-03	fail	NA
4.5	20	8.01E-03	fail	NA
5.0	21	8.23E-03	NC	NA

CASE38 test system with $\lambda = 4$ is considered to analyze the effect of β. In conventional BFS algorithm, the variation in the magnitude of bus voltages of the system is highly oscillating in initial iterations and this oscillation is gradually damped out in later iterations as shown in figure 4.10-(a). It is clearly seen from the figure 4.10-(a) that the voltage magnitude of bus 35 highly oscillates in the initial iterations and as iteration increases, this oscillation damps out gradually. The parameter β is used to adjust the length of voltage correction vector ($[\triangle \mathbf{V}]^{k+1} = [\mathbf{V}]^k - [\mathbf{V}_{ref}] + [\mathbf{BCBV}][\mathbf{I}_{ij}]$) to damp out the oscillation in voltage magnitude. The convergence of the voltage magnitude of bus 35 of the CASE38 test system is shown in figure 4.10 for different values of β ($\beta = 0.5, 0.6, 0.7, 0.8, 0.9$). It is clearly seen from the figure 4.10 that the oscillation in voltage magnitude can be damped out quickly by taking the value of β smaller than 1. As the value of β decreases, the damping in oscillation in the voltage magnitude increases. However, the very low value of β increases the convergence time (settling time). Therefore, the value of β must be set carefully to provide the trade-off between the oscillation and convergence time. In this work, the value of β is chosen 0.5, which provides the balance between oscillation and convergence time in most of the case studies.

4.5 Application of Proposed Approach for DG Modeling and Frequency Update in NTR and MNR

As discussed in the previous subsection, the robustness of NTR and CINR is similar but the NTR algorithm cannot be applied to the systems having (i) DGs with mixed droop characteristics, (ii) DG with isochronous mode of operation and (iii) coupling between the lines. In this work, these issues of NTR are addressed and a new DG model and procedure for updating operating frequency are proposed. These procedures are in general structure and can also be employed with NTR to improve the versatility of the algorithm. In this section, to observe the versatility of the NTR, the modified algorithm is implemented on different types of DCIMGs.

4.5.1 Significance of Proposed DG Model in NTR

The proposed DG model is implemented in NTR by modifying the non-linear equations used in [56]. These non-linear equations are modified in line with the equations proposed in this work. The modified NTR, named NTR-pDMm, can perform the power flow analysis for different cases (discussed in section 4.3.5). The accuracy of the obtained solution of NTR-pDMm is similar to the obtained solution of CINR for all the cases. However, computation time is still the issue in the NTR-pDMm due to the high complexity of the steps of the conventional Newton-Trust algorithm. The results obtained using the proposed DG model in NTR (NTR-pDGm) and CINR in terms of execution time are shown in Table 4.12. It is found that the computation time to converge on a steady-state value in CINR is less than the NTR-pDGm due to the low complexity of the steps required in CINR.

It can be concluded from the above result and discussion that the proposed DG model can be implemented on other Newton-based algorithms to improve their versatility. Also, the convergence rate of CINR is better than modified NTR (NTR-pDGm) due to its simple steps.

Table 4.12: Computation time required to solve power flow for different cases considering CINR, NTR-pDGm algorithm. (NC: Not Converged, CT: Computation Time, %: Percentage improvement in computation time.)

System	Cases	CINR	NTR-pDGm	
		CT(s)	CT(s)	%
CASE22	2	5.58E-03	1.79E-02	220.84
	3	4.22E-03	1.97E-02	365.86
	4	3.81E-03	1.73E-02	353.31
CASE38	2	1.42E-02	3.50E-02	147.17
	3	2.28E-02	3.53E-02	54.77
	4	2.36E-02	4.41E-02	87.21
CASE69	2	1.72E-02	1.40E-01	716.45
	3	1.82E-02	1.38E-01	658.41
	4	1.81E-02	1.50E-01	729.12
CASE160	2	4.99E-02	6.39E-01	1178.58
	3	4.47E-02	5.27E-01	1078.50
	4	6.03E-02	5.20E-01	763.13

4.5.2 Significance of Proposed Frequency Update Procedure in NTR and MNR

The approach taken in the present work is further reinforces its superiority by applying modification in MNR and NTR (MNR-mod and NTR-mod). The modifications made are in line with the approach considered in this paper. For the systems with coupling between the lines, the derivative of admittance matrix cannot be calculated analytically as there is no explicit expression. However, the derivatives of the elements of admittance matrix can be calculated using finite differences method. The frequency terms which are embedded in the elements of the admittance matrix are removed (assuming frequency to be constant). However, the updation of frequency is performed in the outer loop as shown in figure (4.1). The results obtained using proposed modifications in MNR and NTR (MNR-mod and NTR-mod) are shown in table (4.13). The table (4.13) also depicts the results when the elements of Jacobian are calculated using finite differences method (MNR-fd and

NTR-fd). The table (4.13) indicates that significant reduction in computation time can be achieved when the modification are done as per the proposed approach as compared to those obtained using their corresponding finite difference version viz MNR-fd and NTR-fd. further, Table 4.13 also shows that CINR is faster than MNR-mod and NTR-mod, establishing that even if MNR, NTR is adopted for the framework proposed in this work, the CINR outperforms.

Table 4.13: Computational effort of MNR-mod, MNR-fd, NTR-pr, NTR-fd, and CINR for solving different test cases. (iter: number of iterations, CT: Computation Time)

Test Cases	MNR-mod		MNR-fd		NTR-mod		NTR-fd		CINR	
	iter	CT(s)	iter	CT(s)	iter	CT(s)	iter	CT(s)	iter	CT(s)
CASE22	33	0.0205	3	0.3246	37	0.0198	4	0.2932	27	0.0049
CASE33	39	0.0372	3	0.6091	34	0.0297	4	0.5682	24	0.0063
CASE69	37	0.1666	4	0.9351	39	0.1433	5	0.8702	28	0.0133
CASE160	34	0.577	4	3.0717	32	0.5482	4	2.8126	25	0.0608
CASE1458	35	3.656	5	8.2825	37	3.2735	6	7.6835	27	0.3852
CASE3139	38	7.9334	5	17.9729	35	7.1374	6	16.673	29	0.8257

4.6 Summary

In this chapter, a nested-iterative approach, CINR and NBFS are proposed to obtain the power flow solution of droop-based islanded microgrid. A loop-based approach is employed to update the system frequency and voltage of the angle reference bus after every iteration. To analyze the effectiveness of CINR and NBFS, the algorithms are implemented on several test systems including CASE6, CASE22, CASE38, CASE69 and CASE160. In each case study, the load dependency and droop characteristics of DGs are considered. The solutions obtained from the proposed CINR and NBFS are analysed and compared with the solutions obtained from MNR, NTR, DBFS, MBFS and PSCAD. It is found that the solutions obtained from CINR and NBFS show superior convergence in comparison to MNR, NTR, DBFS, MBFS and PSCAD.

Furthermore, the efficacy and robustness of the proposed technique are also analyzed by modifying the operational conditions of DCIMG from well-conditioned to ill-

conditioned by changing the r/x ratio of the lines and the loading conditions. The proposed algorithms converge under various ill-conditions. The proposed techniques also show superior performance in terms of computational time and accuracy in comparison to the performance of NTR and MNR methods of PF analysis.

The effectiveness of the proposed algorithm is also analyzed for the PF analysis of more complicated DCIMG system after considering the isochronous operation of one of the DG in the system. The proposed algorithms also converge for the isochronous operation of the DCIMG. Since, CINR and NBFS are conventional techniques to solve power flow of distribution system, so modeling of different type of droop buses is also considered. The main contributions of proposed approach are as follows:

1. The proposed algorithms, CINR and NBFS, deal with the issues and limitations related to the Newton-based algorithms including MNR and NTR. It also deals with the need of a gradient of the bus admittance matrix with respect to the system frequency in the Jacobian matrix.

2. The proposed algorithms update the system frequency in every loop without using the gradient of the bus admittance matrix or any other variable with respect to the system frequency.

3. A closed loop formulation is proposed to evaluate the values of voltage magnitude of the AR bus and system frequency, which results in fast convergence in the algorithm.

4. The proposed algorithms also converge for the isochronous mode of operation of DCIMG systems.

5. In the proposed approach, DG model and procedure for updating the system frequency is utilized in NTR and MNR to improve its versatility.

The algorithms show rigid convergence characteristics for various conditions of DCIMG. The performance of the proposed algorithms are better in comparison to NTR and MNR approach in terms of computation time and applicability under various operating conditions. Testing of the proposed algorithms on unbalanced DCIMG systems may be the scope of future work.